A Review on Current Reference Calculation of Three-Phase Grid-Connected PV Converters under Grid Faults

[1]Ehsan Afshari, [2]Gholam Reza Moradi, [3]Yongheng Yang, [4]Babak Farhangi, [2]Shahrokh Farhangi

[1]Department of Electrical and Computer Engineering, Northeastern University, Boston, MA
[2]Department of Electrical and Computer Engineering, University of Tehran, Tehran, Iran
[3]Department of Energy Technology, Aalborg University, Aalborg, Denmark
[4]Current Ways Inc, Los Angeles, CA

Abstract—**Unbalanced grid voltage dips may lead to unbalanced non-sinusoidal current injections, dc-link voltage oscillations, and active and/or reactive power oscillations with twice the grid fundamental frequency in three-phase grid-connected Photovoltaic (PV) systems. Double grid frequency oscillations at the dc-link of the conventional two-stage PV inverters can further deteriorate the dc-link capacitor, which is one of the most life-limiting components in the system. Proper controls of these converters may efficiently address this problem. In those solutions, Current Reference Calculation (CRC) is one of the most important issues that should be coped with for a reliable operation of grid-connected converters under unbalanced grid faults. Accordingly, this paper reviews the existing CRC methods and presents a current reference generation method, which can have 16 unique modes. Issues are also investigated in this paper that the two-stage three-phase converter faces in each mode. The performance of the CRC method is verified and compared to the prior-art methods by simulations under unbalanced voltage dips.**

Index Terms—**power oscillation, Current limitation, Dc-link voltage oscillation, Low-Voltage Ride-Through (LVRT), Photovoltaic (PV) systems, Two-stage PV inverter;**

I. INTRODUCTION

Power electronics is a key for the integration of renewable energy systems [1-9]. With an increasing adoption of grid-connected Photovoltaic (PV) systems, a strong emphasis is placed on their dynamic behaviors and impacts on the public grid [10-17]. Accordingly, most countries have revised their grid codes to utilize this huge capacity to improve the grid stability during grid faults [18, 19]. These new requirements enforce distributed generation systems to remain connected to the grid and inject reactive power to the grid under fault incidents [20-24]. Up to now, a vast array of technical literature has been presented on the performance of wind turbines under grid faults [25, 26]. These issues are now gaining more considerations in PV systems [27-32], as the power capacity of an individual PV system is also increasing. Detection of voltage sags, current limitation, current reference calculation, active and reactive power oscillation, and dc-link voltage oscillation are among the important issues. In addition, they are the key issues to a proper operation of grid-connected PV converters under faults [33]. Among them, the Current Reference Calculation (CRC) plays the most impressive role to satisfy the grid requirements, especially under unbalanced grid faults.

Different CRC methods can be found in the literature. In [34], the Instantaneous Active Reactive Control (IARC) has been proposed. The IARC controls three-phase voltages and does not use the Positive Sequence (PS) and Negative Sequence (NS) voltages. Despite of good performance under balanced faults, in case of unbalanced voltage sags, the IARC control strategy leads to non-sinusoidal output currents with a high Total Harmonic Distortion (THD). In [27], the Average Active-Reactive Control (AARC) has then been proposed to mitigate high order harmonics from the IARC method. However, if both active and reactive current are injected, active power suffers from oscillations of twice the fundamental frequency. Hence, the Positive and Negative Sequence Compensation (PNSC) has been introduced to inject sinusoidal PS and NS currents to the grid [34]. However, in case of injecting both active and reactive power, double the grid fundamental frequency oscillations during unbalanced grid faults will appear. Furthermore, the Balanced Positive Sequence Control (BPSC) method is presented in [35] to inject a set of balanced and sinusoidal currents with PS components. Unfortunately, the active and reactive power also have oscillatory components. In [36], a control scheme has been presented which injects both PS and NS proportional to a certain adjustable parameter according to the grid fault severity. As observed from the above, the prior-art control methods suffer from either active power and dc-link voltage oscillations or injection of non-sinusoidal currents into the grid under unbalanced grid faults.

In this paper, the CRC issues are investigated for three-phase grid-connected PV systems under grid faults. A general CRC method is introduced which benefits from four parameters to adjust the oscillation of the active and reactive power under unbalanced faults. Each parameter can have two values, which would lead to 16 unique operational modes. A benchmarking is performed on the operation of these modes. Results are compared to the prior-art CRC methods in terms of active and reactive power oscillations, dc-link voltage oscillations, output current THDs, and output current RMS values. The rest of this paper is organized as following: in Section II, the steady state operation of two stage grid-connected PV system is analyzed for both normal and abnormal conditions. In Section III, a CRC method for the investigated system is proposed and presented in details. Finally, simulations verify the proposed CRC method before the conclusion.

II. PROBLEM FORMULATION

Fig. 1 shows the schematic of a three-phase two-stage grid-connected PV system. The formulation is performed in the Stationary Reference Frame (SRF) transformed from the three-phase system as

$$v_{\alpha\beta} = \begin{bmatrix} v_\alpha \\ v_\beta \end{bmatrix} = \sqrt{\frac{2}{3}} \begin{bmatrix} 1 & -1/2 & -1/2 \\ 0 & \sqrt{3}/2 & -\sqrt{3}/2 \end{bmatrix} \begin{bmatrix} v_a \\ v_b \\ v_c \end{bmatrix} \quad (1)$$

where v_α, v_β are the transformed voltages in the SRF on the α- and β-axis, respectively, and v_a, v_b, v_c are grid voltage vectors. It can be written for current vectors as well. The apparent power (S) can be written as

$$S = v_{\alpha\beta} \cdot i_{\alpha\beta}{}^* = (v_{\alpha\beta}^+ + v_{\alpha\beta}^-) \cdot (i_{\alpha\beta}^+ + i_{\alpha\beta}^-)^* = v_{\alpha\beta}^+ \cdot i_{\alpha\beta}^+{}^* + v_{\alpha\beta}^+ \cdot i_{\alpha\beta}^-{}^* + v_{\alpha\beta}^- \cdot i_{\alpha\beta}^+{}^* + v_{\alpha\beta}^- \cdot i_{\alpha\beta}^-{}^* \quad (2)$$

with $v_{\alpha\beta}^+$ and $v_{\alpha\beta}^-$ being transformed from the following

$$v_{\alpha\beta}^+ = \frac{1}{2} \begin{bmatrix} 1 & -q \\ q & 1 \end{bmatrix} v_{\alpha\beta} \quad (3)$$

$$v_{\alpha\beta}^- = \frac{1}{2} \begin{bmatrix} 1 & q \\ -q & 1 \end{bmatrix} v_{\alpha\beta} \quad (4)$$

in which $q = e^{-j\pi/2}$ is the phase-shifting operator applied on the time domain. $i_{\alpha\beta}^+$ and $i_{\alpha\beta}^-$ can be achieved similarly following the transfer functions in (3) and (4). As seen in (2), there are four terms in the apparent power, one of which can be written as

$$v_{\alpha\beta}^+ \cdot i_{\alpha\beta}^+{}^* = (v_\alpha^+ + j v_\beta^+) \cdot (i_\alpha^+ + j i_\beta^+)^* = v_\alpha^+ i_\alpha^+ + v_\beta^+ i_\beta^+ + j(v_\beta^+ i_\alpha^+ - v_\alpha^+ i_\beta^+) \quad (5)$$

The other three terms can also be achieved. Multiplication of any two terms with the same sequence leads to a constant term in active and reactive power. In contrast, the oscillating part of active and reactive power is caused by the multiplication of any two terms with inverse sequences as

$$P = P_0 + \tilde{P} \quad (6)$$
$$P_0 = v_\alpha^+ i_\alpha^+ + v_\beta^+ i_\beta^+ + v_\alpha^- i_\alpha^- + v_\beta^- i_\beta^- \quad (7)$$
$$\tilde{P} = v_\alpha^+ i_\alpha^- + v_\beta^+ i_\beta^- + v_\alpha^- i_\alpha^+ + v_\beta^- i_\beta^+ \quad (8)$$
$$Q = Q_0 + \tilde{Q} \quad (9)$$
$$Q_0 = v_\beta^+ i_\alpha^+ - v_\alpha^+ i_\beta^+ + v_\beta^- i_\alpha^- - v_\alpha^- i_\beta^- \quad (10)$$
$$\tilde{Q} = v_\beta^+ i_\alpha^- - v_\alpha^+ i_\beta^- + v_\beta^- i_\alpha^+ - v_\alpha^- i_\beta^+ \quad (11)$$

where P and Q are the total active and reactive power, P_0, Q_0, $\tilde{P}$, and $\tilde{Q}$ are the constant and oscillating parts in active and reactive power, respectively. Under unbalanced faults, the NS components will appear in three-phase voltages and currents. Therefore, the active and/or reactive power may present oscillatory components. This issue depends on the current references that are generated by the control algorithm.
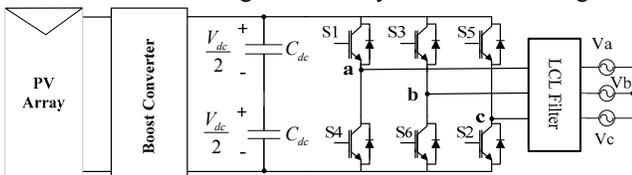

Fig. 1. Three-phase two-stage transformerless grid-connected PV system.

The goal of grid-connected PV systems is to inject all the dc power generated by the PV panels to the grid. This is the reason why Maximum Power Point Tracking (MPPT) methods are employed in such systems. However, in case of grid faults, the control should be modified. The capacitive dc-link in the system operates as an interface. The dc-link capacitor receives the dc power from the PV arrays and instantly injects all the dc power to the ac system. In fact, the dc-link controller balances the power that is delivered to the link and the power that the link is injecting. As a consequence, in case that the active power injected by the inverter is different than the power generated by the PV panels, the dc-link voltage will not remain constant. It means in case that the active power injected to the grid by the inverter starts fluctuating, the dc-link voltage would also oscillate with the same frequency (i.e., twice the grid fundamental frequency). The oscillations in the dc-link voltage (on the capacitor) has a serious impact on the reliable operation of the capacitive dc-link, which is a weak point in two-stage PV inverters [37-40].

III. CONTROL SCHEME

In this section, the proposed CRC method is explained and the features for each mode are studied. Finally, the control block diagram will be illustrated.

A. Proposed General CRC Method

For elimination of the active power oscillations, (7) must be equal to zero. P_{ref} and Q_{ref} are the average value of the active and reactive power references. A general formulation for the calculation of the sinusoidal currents to deliver a certain amount of active and reactive power is proposed as

$$i_{\alpha P} = \frac{v_\alpha^+ - v_\alpha^-}{(v_\alpha^{+2} + v_\beta^{+2}) + k_{\alpha P}(v_\alpha^{-2} + v_\beta^{-2})} P_{ref} \quad (12)$$

$$i_{\beta P} = \frac{v_\beta^+ - v_\beta^-}{(v_\alpha^{+2} + v_\beta^{+2}) + k_{\beta P}(v_\alpha^{-2} + v_\beta^{-2})} P_{ref} \quad (13)$$

$$i_{\alpha Q} = -\frac{v_{\alpha\perp}^+ + v_{\alpha\perp}^-}{(v_{\alpha\perp}^{+2} + v_{\beta\perp}^{+2}) + k_{\alpha Q}(v_{\alpha\perp}^{-2} + v_{\beta\perp}^{-2})} Q_{ref} \quad (14)$$

$$i_{\beta Q} = -\frac{v_{\beta\perp}^+ + v_{\beta\perp}^-}{(v_{\alpha\perp}^{+2} + v_{\beta\perp}^{+2}) + k_{\beta Q}(v_{\alpha\perp}^{-2} + v_{\beta\perp}^{-2})} Q_{ref} \quad (15)$$

$$\begin{bmatrix} v_{\alpha\perp} \\ v_{\beta\perp} \end{bmatrix} = \begin{bmatrix} 0 & -1 \\ 1 & 0 \end{bmatrix} \begin{bmatrix} v_\alpha \\ v_\beta \end{bmatrix} \quad (16)$$

where $i_{\alpha P}$ and $i_{\beta P}$ are the active currents in the SRF, $i_{\alpha Q}$ and $i_{\beta Q}$ are the reactive currents in the SRF, $v_{\alpha\perp}$ and $v_{\beta\perp}$ are the orthogonal version of the SRF voltage vectors, $k_{\alpha P}$, $k_{\beta P}$, $k_{\alpha Q}$, and $k_{\beta Q}$ are the key parameters which can be either +1 or -1 to adjust the active and reactive current references in the SRF regarding grid requirements. As mentioned previously, the purpose of this paper is to calculate the current references such that the active power does not include oscillatory components. Therefore, among these modes, only four modes have this feature, which is provided in Table I.

TABLE I.
CONTROL MODES WITH NO ACTIVE POWER OSCILLATION.

Mode	$k_{\alpha P}$	$k_{\beta P}$	$k_{\alpha Q}$	$k_{\beta Q}$
Mode 1	+1	+1	+1	+1
Mode 2	-1	-1	-1	-1
Mode 3	+1	+1	-1	-1
Mode 4	-1	-1	+1	+1

B. Implementation of the Control Scheme

The control structure consists of two stages which can operate independently due to the capacitive dc-link that decouples these two stages. The first stage, which is a dc-dc converter operates as a MPPT controller. The second stage is a Full Bridge (FB) three-phase inverter which converts the dc power to ac power. A Proportional Integral (PI) controller is adopted for the dc-link to regulate the dc voltage. The output of the PI controller determines the active power that should be delivered into the gird, in order to adjust the dc-link voltage. Two Proportional Resonant (PR) controllers are adopted for controlling the injected currents in the SRF [41]. The reactive reference Q^* is calculated based on the grid requirements, once voltage sag is occurred.
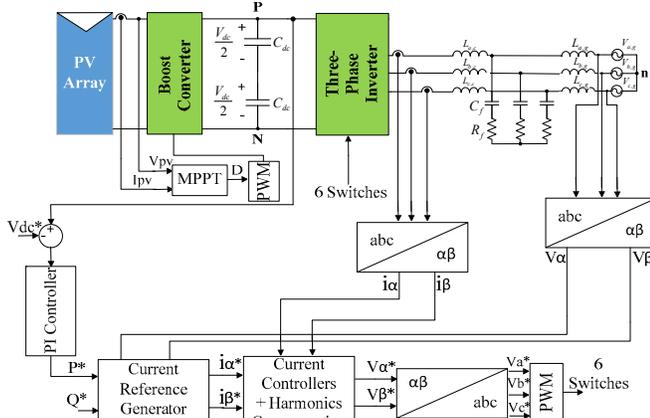
Fig. 2. Control block diagram of the two-stage three-phase grid-connected PV system, where the proposed current reference calculation scheme can be implemented in the "Current Reference Generator" block.

IV. BENCHMARKING (SIMULATION RESULTS)

A simulation testbed is designed in MATLAB/SIMULINK platform to verify the performance of the proposed CRC for each mode and also to compare with the prior-art CRC methods. Table II shows the system parameters. This case study is an unbalanced voltage sag fault case. In this scenario, the phase-b and phase-c voltages V_b and V_c fall to 0.5 per-unit at t = 0.2 s and then recover to the nominal value at t = 0.3 s. Fig. 3 shows the profiles of the three-phase grid voltages for the case study.

A. Proposed CRC Method

Fig. 4 shows the injected currents at the moment of the fault for the two-stage PV system with the proposed CRC method. It is observed in Fig. 4 that because of the unbalanced fault, the phase-b and phase-c currents are increased more than the other phase. The Root Mean Square (RMS) value of the phase-c current is equal to 5.85 A with the THD of 1.48% during the

fault in this case. Fig. 5(a) and (b) illustrate the dc-link voltage and active power waveforms, which do not have significant oscillatory components during the unbalanced fault. Fig. 5(c) shows the injected reactive power, which has oscillations of twice the grid fundamental frequency as expected based on the discussion in Section III.

TABLE II.
POWER CONVERTER PARAMETERS OF THE THREE-PHASE GRID-CONNECTED PV SYSTEM.

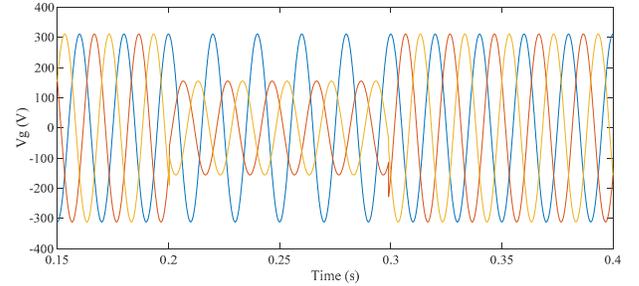| Parameters	Value
Nominal Power	2000 W
Grid line-Line voltage (RMS)	380 V
Grid frequency	50 Hz
Boost input inductor	6.5 mH
Inverter side inductance of the LCL filter	6.5 mH
Grid side inductance of the LCL filter	0.65 mH
Capacitance of the LCL filter	2.2 µF
Switching frequency	16000 Hz
dc-link capacitor (two in series)	680 µF

Fig. 3. Three-phase grid voltages for the two-stage grid-connected PV system.
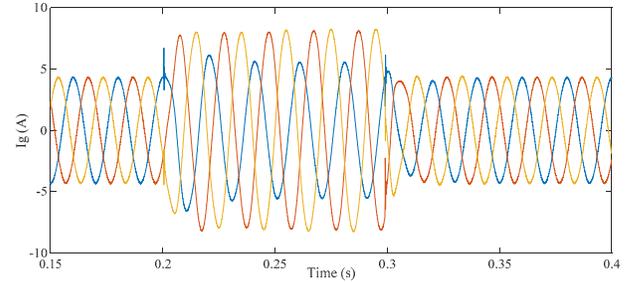

Fig. 4. Three-phase injected currents of the two-stage PV system under the unbalanced fault using the proposed CRC method (Mode 1).
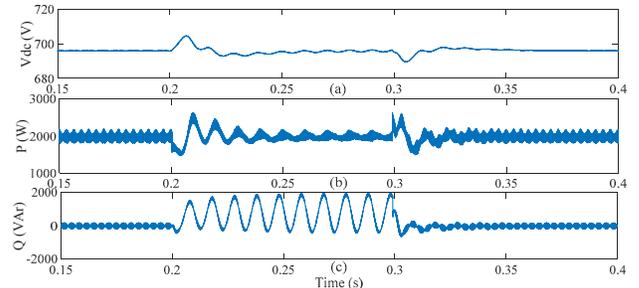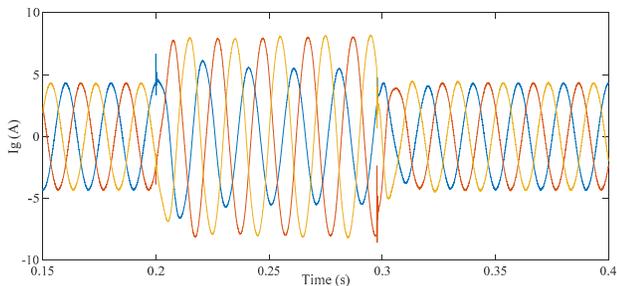

Fig. 5. Performance of the three-phase grid-connected PV system under the unbalanced grid fault using the proposed CRC method (Mode 1): (a) the dc-link voltage, (b) the injected active power, and (c) the injected reactive power.

Fig. 6 depicts the injected currents during the fault using the proposed general CRC method (Mode 2). In this mode, the RMS value of the phase-c current is equal to 5.79 A with the THD of 1.36%. Fig. 7 depicts the dc-link voltage and active power waveforms in which the DGF oscillation is lowered. In

addition, Fig. 8 depicts the injected three-phase currents using mode 3 in which the phase-c current RMS value is equal to 5.8 A with the THD of 1.32%. Fig. 9 represents the dc-link voltage, active power, and reactive power waveforms, which are the same as in Mode 1 and 2. Furthermore, Fig. 10 illustrates the three-phase injected currents using Mode 4. In this mode, the phase-c current has the RMS value of 5.86 A with the THD of 1.43%. This mode produces the highest amplitude of the phase-c current. As expected, the dc-link voltage, active power, and reactive power waveforms are the same as in Mode 1, 2, and 3, as depicted in Fig. 11. As can be seen, in all four modes, the phase-c current is increased more than the other phases.

Fig. 6. Three-phase injected currents of the two-stage PV system under the unbalanced fault using the proposed CRC method (Mode 2).
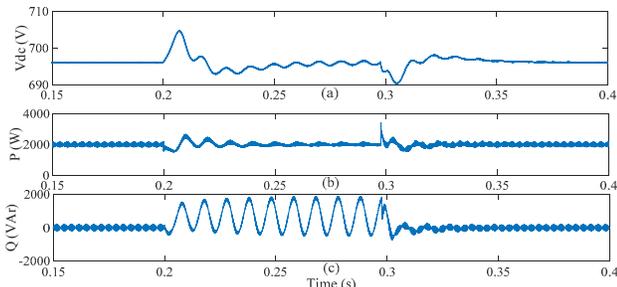

Fig. 7. Performance of the three-phase grid-connected PV system under the unbalanced grid fault using the proposed CRC method (Mode 2): (a) the dc-link voltage, (b) the injected active power, and (c) the injected reactive power.
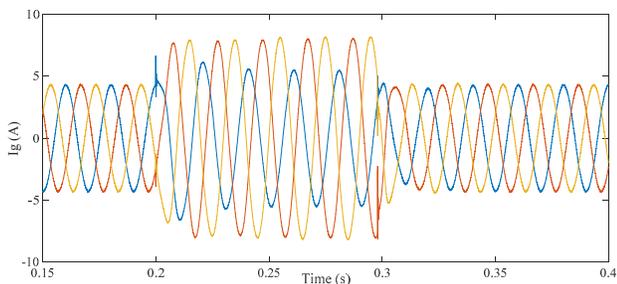

Fig. 8. Three-phase injected currents of the two-stage PV system under the unbalanced fault using the proposed CRC method (Mode 3).
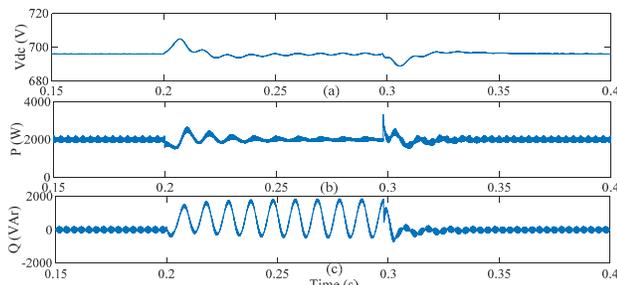

Fig. 9. Performance of the three-phase grid-connected PV system under the unbalanced grid fault using the proposed CRC method (Mode 3): (a) the dc-link voltage, (b) the injected active power, and (c) the injected reactive power.
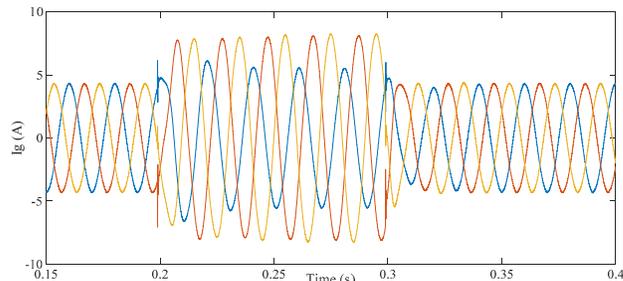

Fig. 10. Three-phase injected currents of the two-stage PV system under the unbalanced fault using the proposed CRC method (Mode 4).
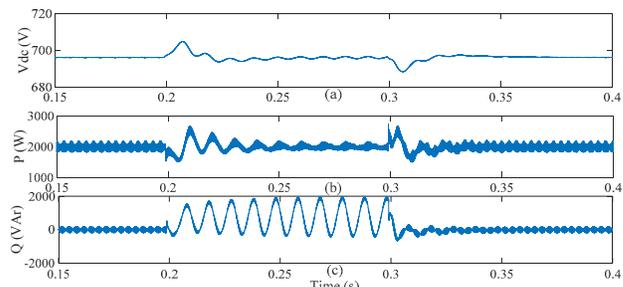

Fig. 11. Performance of the three-phase grid-connected PV system under the unbalanced grid fault using the proposed CRC method (Mode 4): (a) the dc-link voltage, (b) the injected active power, and (c) the injected reactive power.

B. PNSC Method

Fig. 12 represents the injected three-phase currents when the PNSC method is employed. As shown, the phase-b current is increased more than the other phases and its RMS value is equal to 6.29 A with the THD value of 2.12%. The dc-link voltage and the injected active power contain significant oscillatory components using the PNSC as it is shown in Fig. 13(a) and (b), which contrasts with the proposed CRC method as presented in the above. Moreover, as depicted in Fig. 13(c), the injected reactive power with the PNSC method also includes large oscillations of twice the grid fundamental frequency.
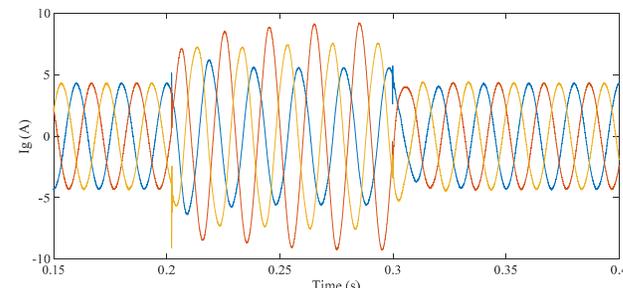

Fig. 12. Three-phase injected currents of the two-stage PV system under the unbalanced fault using the PNSC method.
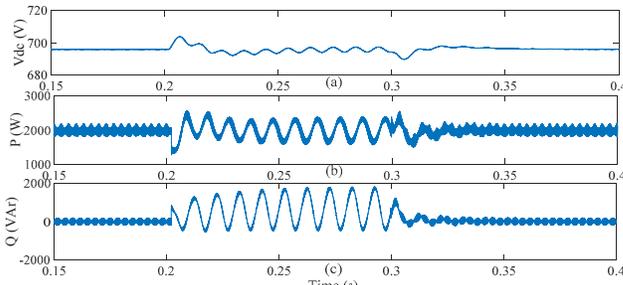

Fig. 13. Performance of the three-phase grid-connected PV system under the unbalanced grid fault using the PNSC method: (a) the dc-link voltage, (b) the injected active power, and (c) the injected reactive power.

C. AARC Method

Fig. 14 illustrates the injected three-phase currents when using the AARC method. According to Fig. 14, the phase-a current is increased more than the other phases and its RMS value is equal to 5.46 A with the THD value of 1.59%. Moreover, the dc-link voltage and the injected active power contains large oscillatory components when the AARC is adopted, as shown in Fig. 14(a) and (b), compared to the proposed CRC method in different modes. However, as depicted in Fig. 15(c), the injected reactive power has a constant value without such significant double the grid fundamental frequency oscillations.
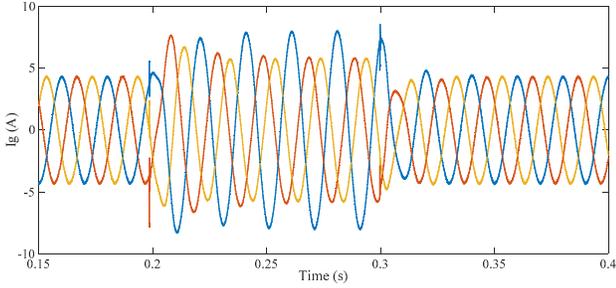

Fig. 14. Three-phase injected currents of the two-stage PV system under the unbalanced fault using the AARC method.
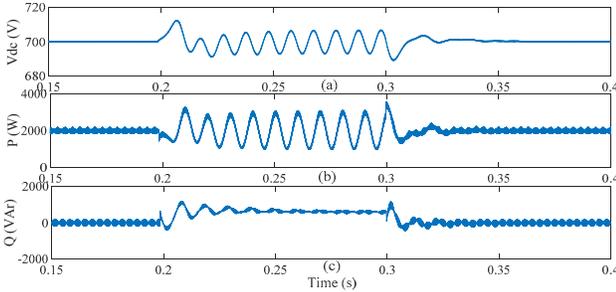

Fig. 15. Performance of the three-phase grid-connected PV system under the unbalanced grid fault using the AARC method: (a) the dc-link voltage, (b) the injected active power, and (c) the injected reactive power.

D. BPSC Method

Fig. 16 depicts the injected three-phase currents with the BPSC method. According to Fig. 16, all currents are increased equally and they are balanced which is one of the features of this method. The RMS value is equal to 4.83 A with the THD value of 1.7%. Although the injected currents are balanced and sinusoidal, active and reactive power and dc-link voltage suffer from large oscillations as it can be observed in Fig. 17 in contrast to the proposed method. The large oscillations has a double the grid fundamental frequency.
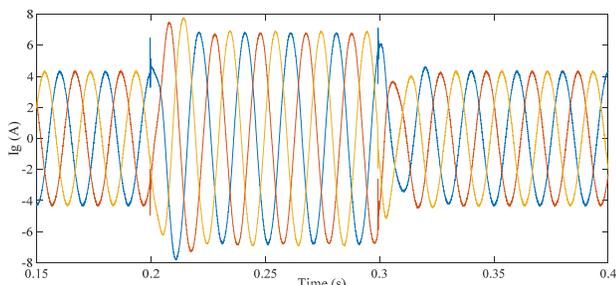

Fig. 16. Three-phase injected currents of the two-stage PV system under the unbalanced fault using the BPSC method.
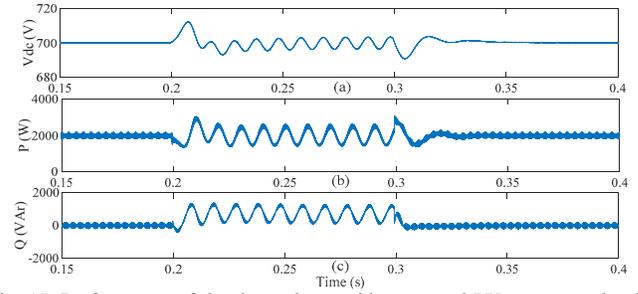

Fig. 17. Performance of the three-phase grid-connected PV system under the unbalanced grid fault using the BPSC method: (a) the dc-link voltage, (b) the injected active power, and (c) the injected reactive power.
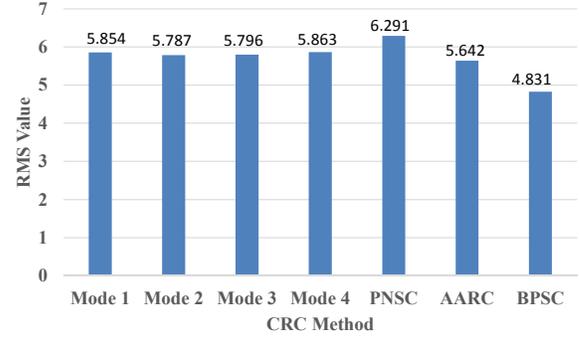

Fig. 18. RMS value (A) of the highest injected phase-current for all the CRC methods under the unbalanced fault. Among four modes of proposed CRC method, Mode 4 and Mode 2 produce the highest and lowest RMS values, respectively.
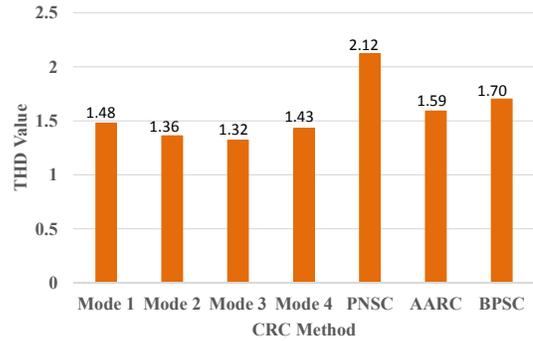

Fig. 19. THD value (%) of the highest injected phase-current for all the CRC methods under the unbalanced fault. Mode 2 and Mode 3 of the proposed general CRC method have the lowest THD value, while the PNSC has the highest. All modes of the proposed general CRC method give lower THD values compared to the prior-art solutions.

E. Benchmarking of the CRC Methods

As depicted in Fig. 18, among the four modes of the proposed CRC method, Mode 4 produces the highest RMS value of the phase-c current whereas Mode 2 produces the lowest one. Totally, the PNSC generates the highest RMS value with the worst THD, as it is compared in Fig. 19. Only the BPSC method can inject balanced sinusoidal three-phase currents with the lowest RMS value, which can be observed in Fig. 18. The reason is that all three-phase currents are increased equally. However, the active and reactive power and dc-link voltage suffer from large DGF oscillations in this method, as it has been presented in Fig. 17.

Furthermore, Table III summarizes the performance of each CRC method during the unbalanced grid fault. It can be seen in Table III that the AARC has the second lowest RMS value.

However, the dc-link voltage and injected active power have large oscillations of twice the grid fundamental frequency with a high peak-peak value, which is totally in contrast to the proposed CRC method. In addition, the PNSC method has the lowest active power oscillations among the other methods. However, it cannot eliminate the double grid fundamental frequency oscillations in the active power and the dc-link voltage, as it is also evidenced in Fig. 13. Among all these methods, only the proposed CRC method has almost fully eliminated the oscillations of twice the grid-fundamental frequency in the active power and dc-link voltage. Moreover, these four modes of the proposed CRC method can inject three-phase currents with the lowest THD, as it can be observed in Fig. 19 and Table III.

TABLE III.
THD AND RMS VALUES OF HIGHEST INJECTED PHASE-CURRENT OF THE TWO-STAGE GRID-CONNECTED PV SYSTEM UNDER THE UNBALANCED GRID FAULT WITH DIFFERENT CRC METHODS.

CRC Method	RMS Value (A)	THD Value %	Active power and dc-link voltage oscillation	Reactive power oscillation
Mode 1	5.854	1.48	No	Yes
Mode 2	5.787	1.36	No	Yes
Mode 3	5.796	1.32	No	Yes
Mode 4	5.863	1.43	No	Yes
PNSC	6.291	2.12	Yes (Low)	Yes
AARC	5.642	1.59	Yes	No
BPSC	4.831	1.7	Yes	Yes

V. CONCLUSION

This paper has explored the CRC methods for three-phase grid-connected PV power converters during unbalanced grid faults. The proposed CRC method has 16 unique modes, four of which have the capability to eliminate the double grid fundamental frequency oscillations in both the active power and the dc-link voltage as verified by the simulation results in this paper. This feature is the most important advantage of this general CRC method under unbalanced grid faults. In contrast, in the prior-art solutions including BPSC, PNSC, and AARC methods, the active power and the dc link voltage include significant oscillatory components under unbalanced grid faults. Although the oscillation amplitude of the active power using the PNSC scheme is low, the injected currents have the highest RMS value which can be a severe problem for implementation of a current limiting. Among the four modes of the proposed general CRC method, Mode 4 produces the highest RMS value of the current with the THD of 1.43%. Since the overcurrent failure must be prevented in the operation of grid-connected converters under faults, Mode 2 with the lowest RMS value of current is more promising. This mode can inject three-phase currents with the THD of 1.36% under faults.

REFERENCES

[1] S. Ouni, M. R. Zolghadri, M. khodabandeh, M. Shahbazi, J. Rodriguez, H. O. Mirzamani, *et al.*, "Improvement of Post-Fault Performance of Cascaded H-bridge Multilevel Inverter," *IEEE Transactions on Industrial Electronics,* vol. PP, no. 99, pp. 1-1, 2016.

[2] B. Farhangi and S. Farhangi, "Application of Z-source converter in photovoltaic grid-connected transformer-less inverter," *Electrical Power Quality and Utilisation. Journal,* vol. 12, no. 2, pp. 41-45, 2006.

[3] B. Farhangi and S. Farhangi, "Comparison of z-source and boost-buck inverter topologies as a single phase transformer-less photovoltaic grid-connected power conditioner," *a a,* vol. 2, no. 1, p. 32, 2006.

[4] J. Mendoza-Mendoza, J. Renteria-Soto, P. Martinez, G. Vazquez, G. Escobar, and J. Sosa, "A comparative analysis of the 5L-AH6 and 5L-SC topologies for grid-connected transformer-less multilevel inverters for PV systems," in *Power Electronics (CIEP), 2016 13th International Conference on*, 2016, pp. 265-270.

[5] B. Farhangi and H. A. Toliyat, "Piecewise Linear Model for Snubberless Dual Active Bridge Commutation," *IEEE Transactions on Industry Applications,* vol. 51, no. 5, pp. 4072-4078, 2015.

[6] B. Farhangi and H. A. Toliyat, "Modeling and Analyzing Multiport Isolation Transformer Capacitive Components for Onboard Vehicular Power Conditioners," *IEEE Transactions on Industrial Electronics,* vol. 62, no. 5, pp. 3134-3142, 2015.

[7] S. Farhangi, E. Asl-Soleimani, A. Khodayari, and B. Farhangi, "Experimental Investigation of Proper Tilt Angles for Stand-Alone, Irrigation PV Pumping and Grid Connected Application in Tehran," in *Proceedings of ISES World Congress 2007 (Vol. I–Vol. V)*, 2008, pp. 1601-1605.

[8] B. Farhangi and K. Butler-Purry, "Transient study of DC zonal electrical distribution system in next generation shipboard integrated power systems using PSCAD™," in *North American Power Symposium (NAPS), 2009*, 2009, pp. 1-8.

[9] H. Mehrabian-Nejad, S. Mohammadi, and B. Farhangi, "Novel control method for reducing EMI in shunt active filters with level shifted random modulation," in *Power Electronics, Drives Systems & Technologies Conference (PEDSTC), 2015 6th*, 2015, pp. 585-590.

[10] A. Marinopoulos, F. Papandrea, M. Reza, S. Norrga, F. Spertino, and R. Napoli, "Grid integration aspects of large solar PV installations: LVRT capability and reactive power/voltage support requirements," in *PowerTech, 2011 IEEE Trondheim*, 2011, pp. 1-8.

[11] S. Pattnaik, R. Dash, S. C. Swain, and P. Mohapatra, "Control of active and reactive power of a three phase grid connected photovoltaic system," in *2016 International Conference on Circuit, Power and Computing Technologies (ICCPCT)*, 2016, pp. 1-6.

[12] E. Afshari, R. Rahimi, B. Farhangi, and S. Farhangi, "Analysis and modification of the single phase transformerless FB-DCB inverter modulation for injecting reactive power," in *2015 IEEE Conference on Energy Conversion (CENCON)*, 2015, pp. 413-418.

[13] G. R. Moradi, E. Afshari, R. Rahimi, B. Farhangi, and S. Farhangi, "Improvement of the modulation method for single-phase transformerless photovoltaic conergy inverter for reactive power injection capability," in *2016 24th Iranian Conference on Electrical Engineering (ICEE)*, 2016, pp. 1312-1317.

[14] S. Danyali, S. K. M. Niapour, S. Hosseini, G. Gharehpetian, and M. Sabahi, "New Single-Stage Single-Phase Three-Input DC-AC Boost Converter for Stand-Alone Hybrid PV/FC/UC Systems," *Electric Power Systems Research,* vol. 127, pp. 1-12, 2015.

[15] O. M. Arafa, A. A. Mansour, K. S. Sakkoury, Y. A. Atia, and M. M. Salem, "Realization of Single-Phase Single-Stage Grid-Connected PV System," *Journal of Electrical Systems and Information Technology,* 2016.

[16] A. Sangwongwanich, Y. Yang, and F. Blaabjerg, "A Sensorless Power Reserve Control Strategy for Two-Stage Grid-Connected PV Systems," *IEEE Transactions on Power Electronics,* vol. PP, no. 99, pp. 1-1, 2017.

[17] R. Rahimi, B. Farhangi, and S. Farhangi, "New topology to reduce leakage current in three-phase transformerless grid-connected photovoltaic inverters," in *Power Electronics and Drive Systems Technologies Conference (PEDSTC), 2016 7th*, 2016, pp. 421-426.

[18] F. Iov, A. D. Hansen, P. E. Sørensen, and N. A. Cutululis, "Mapping of grid faults and grid codes," Risø National Laboratory 8755036228, 2007.

[19] R. Rahimi, E. Afshari, B. Farhangi, and S. Farhangi, "Optimal placement of additional switch in the photovoltaic single-phase grid-connected transformerless full bridge inverter for reducing common mode leakage current," in *2015 IEEE Conference on Energy Conversion (CENCON)*, 2015, pp. 408-412.

[20] Y. Yang, H. Wang, and F. Blaabjerg, "Reactive Power Injection Strategies for Single-Phase Photovoltaic Systems Considering Grid Requirements," *IEEE Transactions on Industry Applications,* vol. 50, no. 6, pp. 4065-4076, 2014.

[21] G. Ding, F. Gao, H. Tian, C. Ma, M. Chen, G. He, *et al.*, "Adaptive DC-link voltage control of two-stage photovoltaic inverter during low voltage ride-through operation," *IEEE Transactions on Power Electronics,* vol. 31, no. 6, pp. 4182-4194, 2016.

[22] R. Meyer, A. Zlotnik, and A. Mertens, "Fault ride-through control of medium-voltage converters with LCL filter in distributed generation systems," *IEEE Transactions on Industry Applications,* vol. 50, no. 5, pp. 3448-3456, 2014.

[23] Y. Yang, F. Blaabjerg, H. Wang, and M. G. Simoes, "Power control flexibilities for grid-connected multi-functional photovoltaic inverters," *IET Renewable Power Generation,* vol. 10, no. 4, pp. 504-513, 2016.

[24] S. Haghnazari, M. Khodabandeh, and M. R. Zolghadri, "Fast fault detection method for modular multilevel converter semiconductor power switches," *IET Power Electronics,* vol. 9, no. 2, pp. 165-174, 2016.

[25] C. EnergiNet, "Grid connection of wind turbines to networks with voltages below 100 kV," *Regulation TF,* vol. 3, no. 6, 2004.

[26] J. Farhang, M. Eydi, B. Asaei, and B. Farhangi, "Flexible strategy for active and reactive power control in grid connected inverter under unbalanced grid fault," in *2015 23rd Iranian Conference on Electrical Engineering*, 2015, pp. 1618-1623.

[27] J. L. Sosa, M. Castilla, J. Miret, J. Matas, and Y. Al-Turki, "Control strategy to maximize the power capability of PV three-phase inverters during voltage sags," *IEEE Transactions on Power Electronics,* vol. 31, no. 4, pp. 3314-3323, 2016.

[28] Y. Yang, F. Blaabjerg, and H. Wang, "Low-Voltage Ride-Through of Single-Phase Transformerless Photovoltaic Inverters," *IEEE Transactions on Industry Applications,* vol. 50, no. 3, pp. 1942-1952, 2014.

[29] Y. Yang, F. Blaabjerg, and Z. Zou, "Benchmarking of Grid Fault Modes in Single-Phase Grid-Connected Photovoltaic Systems," *IEEE Transactions on Industry Applications,* vol. 49, no. 5, pp. 2167-2176, 2013.

[30] F. A. Neves, M. Carrasco, F. Mancilla-David, G. M. Azevedo, and V. S. Santos, "Unbalanced Grid Fault Ride-Through Control for Single-Stage Photovoltaic Inverters," *IEEE Transactions on Power Electronics,* vol. 31, no. 4, pp. 3338-3347, 2016.

[31] M. Hamzeh, S. Farhangi, and B. Farhangi, "A new control method in PV grid connected inverters for anti-islanding protection by impedance monitoring," in *2008 11th Workshop on Control and Modeling for Power Electronics*, 2008, pp. 1-5.

[32] B. Farhangi, "A novel modified deadbeat controller for vehicle to grid application," in *Power Electronics, Drives Systems & Technologies Conference (PEDSTC), 2015 6th*, 2015, pp. 47-52.

[33] E. Afshari, B. Farhangi, Y. Yang, and S. Farhangi, "A Low-Voltage Ride-Through Control Strategy for Three-Phase Grid-Connected PV Systems " presented at the IEEE Power and Energy Conference at Illinois (PECI), Illinois, USA, 2017.

[34] R. Teodorescu and M. Liserre, *Grid converters for photovoltaic and wind power systems* vol. 29: John Wiley & Sons, 2011.

[35] P. Rodriguez, A. V. Timbus, R. Teodorescu, M. Liserre, and F. Blaabjerg, "Flexible active power control of distributed power generation systems during grid faults," *IEEE Transactions on Industrial Electronics,* vol. 54, no. 5, pp. 2583-2592, 2007.

[36] A. Junyent-Ferre, O. Gomis-Bellmunt, T. C. Green, and D. E. Soto-Sanchez, "Current control reference calculation issues for the operation of renewable source grid interface VSCs under unbalanced voltage sags," *IEEE Transactions on Power Electronics,* vol. 26, no. 12, pp. 3744-3753, 2011.

[37] M. Khodabandeh, M. R. Zolghadri, M. Shahbazi, and N. Noroozi, "T-type direct AC/AC converter structure," *IET Power Electronics,* vol. 9, no. 7, pp. 1426-1436, 2016.

[38] M. Khodabandeh, M. R. Zolghadri, and N. Noroozi, "A new t-type direct AC/AC converter," in *The 6th Power Electronics, Drive Systems & Technologies Conference (PEDSTC2015)*, 2015, pp. 247-252.

[39] S. K. M. Niapour and M. Amirabadi, "Extremely Sparse Parallel AC-Link Universal Power Converters," *IEEE Transactions on Industry Applications,* vol. 52, no. 3, pp. 2456-2466, 2016.

[40] M. Amirabadi, A. Balakrishnan, H. A. Toliyat, and W. C. Alexander, "High-Frequency AC-Link PV Inverter," *IEEE Transactions on Industrial Electronics,* vol. 61, no. 1, pp. 281-291, 2014.

[41] Y. Yang, K. Zhou, and F. Blaabjerg, "Enhancing the Frequency Adaptability of Periodic Current Controllers With a Fixed Sampling Rate for Grid-Connected Power Converters," *IEEE Transactions on Power Electronics,* vol. 31, no. 10, pp. 7273-7285, 2016.